Available online at www.sciencedirect.com

ScienceDirect

Procedia CIRP 100 (2021) 1–6

www.elsevier.com/locate/procedia

31st CIRP Design Conference 2021 (CIRP Design 2021)

# Simulation-based digital twin for the manufacturing of thermoplastic composites

André Hürkamp[a,c,**], Ralf Lorenz[b,c], Tim Ossowski[a,c], Bernd-Arno Behrens[b,c], Klaus Dröder[a,c]

[a]*Technische Universität Braunschweig, Institute of Machine Tools and Production Technology, Langer Kamp 19b, 38106 Braunschweig, Germany*
[b]*Leibniz Universität Hannover, Institute of Forming Technology and Machines, An der Universität 2, 30823 Garbsen, Germany*
[c]*Open Hybrid LabFactory, Hermann-Münch-Straße 2, 38440 Wolfsburg, Germany*

**Abstract**

The bond strength between a thermoformed fibre reinforced thermoplastic sheet and an injected polymer is the limiting factor for the structural integrity of overmoulded thermoplastic composites. In this contribution, a simulation based digital twin of the thermoforming process is presented. From numerical parametric studies a reduced order model based on Proper Orthogonal Decomposition (POD) is developed. The combination with machine learning methods enables the real-time computation of arbitrary physical reliable temperature fields with sufficient accuracy to be used for design purposes and as inline quality gates.



*Keywords:* Thermoplastic Composites; Thermoforming; Finite Element Method; Reduced Order Modelling; Digital Twin

## 1. Introduction

In order to meet environmental goals in future mobility concepts, lightweight design is one of the main factors since it yields a resource efficient use of materials by nature. In particular, weight reduction leads to less energy consumption during the use phase or in case of electrical vehicles, to a range extension, respectively. Regarding the complete life cycle, the production phase already leads to initial environmental impacts (carbon foot print). Therefore, especially for lightweight materials such as fibre reinforced plastics, sophisticated digital design methods for both, the final structure and its production are necessary to meet the requirements regarding structural performance, weight, costs, and environment. In the automotive industry, thermoplastics are already used in many applications since their processing enables efficient manufacturing and short cycle times. Until now, those materials are mainly processed by injection moulding. However, for structural relevant parts, continuous fibre reinforced plastics provide a larger lightweight potential. In the particular case of thermoplastic composites, the process combination of thermoforming and injection moulding illustrated in Fig. 1 allows a relatively high degree of freedom for the design. In this way, shell-shaped structures made of continuous fibre-reinforced thermoplastics (FRTP) can be reinforced with ribs and additional functional elements can be added by overmoulding.

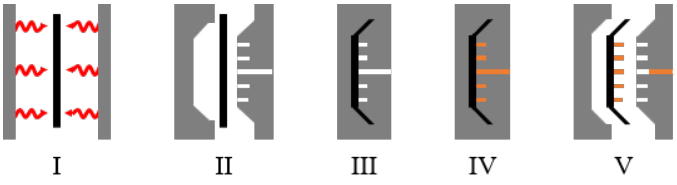


Fig. 1. Process chain for thermoplastic composites overmoulding: (I) Heating, (II) Transfer, (III) Thermoforming, (IV) Overmoulding, (V) Demoulding ; adpated from [1]

In the first step, the FRTP (e.g., organo sheet) is heated up to achieve formability (I). After it is transferred into the mould (II), the FRTP is thermoformed by the movable part of the injection mould (III). The overmoulding process starts directly

* Corresponding author. Tel.: +49 531 391-65044 ; fax: +49 531 391-5842.
*E-mail address:* a.huerkamp@tu-braunschweig.de (André Hürkamp).

2212-8271 
10.1016/j.procir.2021.05.001

afterwards (IV). The injected thermoplastic polymer is compatible with the matrix material of the FRTP sheet and it can either be unfilled or fibre reinforced. After the part has been solidified, it is demoulded (V).

In this process chain, the resulting bond strength between FRTP sheet and injected polymer is the limiting factor. It is mainly influenced by the temperature history [2]. Therefore it is mandatory to take into account the interface conditions during manufacturing. In the literature, different models describe the evolution of the interface bond strength in terms of a healing model [3, 4]. Therein, computer simulations of the melt flow have been used to identify the process conditions at the interface. Besides other parameters such as pressure and viscosity, the temperature at the interface is decisive.

As stated in Fig. 1, the process chain consists of two integrated process steps (III and IV). Hence, the knowledge of the interface temperature during manufacturing is important to ensure a proper bond strength. Thereby, the part and process design plays an important role since flow path and fill time during the overmoulding influence the local interface properties. Due to the existing cavities in the mould, the temperature distribution of the FRTP sheet is inhomogeneous. Furthermore, a relative movement between die and blank occurs, which leads to different contact conditions and to an inhomogenous temperature distribution. Since the temperature at the internal interface can hardly be measured during manufacturing, Hürkamp et al. [5] propose a Cyber Physical Production System (CPPS) based approach for a digital twin using simulation results and machine learning. The approach is adapted from [6] and uses a numerical design of experiments for the data acquisition. Subsequently, machine learning is used to derive a surrogate model that computes the bond strength quality in dependence of the interface temperature during the injection moulding process. This allows a real-time prediction of the parts quality based on arbitrary process settings and the process chain (e.g., waiting times due to failure). In this way, heating cycles, holding times or process temperatures can be controlled during operation.

This paper presents a digital twin framework combining numerical simulations, Proper Orthogonal Decomposition (POD) and Machine Learning. The resulting digital twin of the thermoforming process enables a fast prediction of the temperature field. It can be used during the product development for manufacturing-dependent design optimisation, uncertainty quantification or as input for subsequent injection moulding simulations to optimise the overmoulding. Eventually, the real-time feasibility of the digital twin allows to transfer the knowledge about process and part properties from the design phase into the operation phase (e.g., as inline virtual quality gates).

## 2. Simulation-Based Digital Twin

The development of the digital twin is based on reduced order modelling (ROM). ROM techniques enable online feasible real-time simulations or fast parametric studies for optimisation tasks especially for nonlinear and high-dimensional problems based on physical principles. Thereby, ROM does not simplify the model and the underlying physics [7]. In the context of CPPS, ROM can extend the collected data with physical meaningful structural information computed from surrogate models.

In this contribution, we combine POD [8] with machine learning. During an offline phase a parametric solution of the thermoforming process is computed. In practical applications of product development, those simulations are carried out with specific parameters to optimise process, mould and structural design. By systematically solving the problem within a predefined parameter set, a solid database is obtained to develop online feasible surrogates. Another practical advantage of POD is its quite simple implementation and independence of software packages. The governing physical equations describing the system behaviour are solved by means of numerical methods such as Finite Element Method (FEM). This provides a model-based knowledge and process understanding in contrary to purely data driven (black-box) approaches. Furthermore, ROM by POD preserves the boundary conditions of the underlying physical problem [9]. The method presented here is generally applicable for all types of mechanical models and solvers.

### 2.1. Proper Orthogonal Decomposition

For developing the reduced order model, POD is used in this contribution. For the problem statement, we follow mainly the notation given in [9]. A similar approach has been used for a POD-based ROM of manufacturing processes for multi-material lightweight parts [10].

Let $\mathbf{u}(\mathbf{x}, \mathbf{p})$ be the solution of the given physical problem. It represents the spatial distribution of the solution $\mathbf{u}$ (e.g., temperature) for a given set of input parameters $\mathbf{p}$ at the coordinates $\mathbf{x}$. In the context of POD, $\mathbf{u}$ is referred to as snapshot. In order to provide a sufficient database $n_s$ snapshots are computed. The matrix of snapshots $\mathbf{U}(\mathbf{x}, \mathbf{p}) = [u_1(\mathbf{x}, \mathbf{p}) \dots u_{n_s}(\mathbf{x}, \mathbf{u})]$ contains $n_s$ solution vectors of full-scale simulation. The size of $\mathbf{U}(\alpha)$ is $n_x \times n_s$, where $n_x$ denotes the number of results contained in $\mathbf{u}$. According to [11], computing the eigenvalues from the correlation matrix $\mathbf{R} = \frac{1}{n_s}\mathbf{U}^{\mathrm{T}}\mathbf{U}$ yields $n_s$ eigenvalues $\lambda_i$ and the corresponding eigenvectors $\bar{\phi}_i$. Normalising $\phi_i = \mathbf{U}\bar{\phi}_i / \|\mathbf{U}\bar{\phi}_i\|$ leads to the reduced representation

$$\mathbf{U}^{\alpha}(\mathbf{x}, \mathbf{p}) \approx \sum_{i=1}^{k} \phi_i(\mathbf{x}) \cdot a_i(\mathbf{p}), \tag{1}$$

where $a_i = \phi_i^T \mathbf{u}$ denote the POD coefficients [9] and is referred to as weighting coefficient in the following. The vector $\phi_i(\mathbf{x})$ is denoted as spatial mode and depends only on $\mathbf{x}$. In contrary, the coefficients $a_i(\mathbf{p})$ depend only on the input $\mathbf{p}$. In general, there is no restriction on $\mathbf{p}$. In the present use case it represents the thermoforming process parameters. A reduced representation of the solution is obtained when $k < n_s$ modes are used in the series expansion (1). For $k = n_s$, the exact solution is represented with respect to computer accuracy.

### 2.2. Machine learning

In the reduced solution, the coefficients $a$ depend on the set of process parameters $\mathbf{p}$ given as input. Due to the strong correlation between the input parameters, no interpolation between the functions is possible. Hence, having only the information contained in Eq. (1), combinations of $\mathbf{p}$ that are not contained in the snapshots cannot be predicted. In order to find this map between the coefficients, the approach for a physics-inspired parametrisation using Machine Learning by Swischuk et al. [9] is used. The inputs of each snapshot yield the matrix $P \in \mathbb{R}^{n_s \times n_p}$, where $n_p$ denotes the number of inputs. Accordingly, the coefficients are collected in matrix $A \in \mathbb{R}^{n_s \times k}$. As machine learning method, a decision tree with bootstrap aggregating (bagging) is used. It has been shown, that decision trees are fast in prediction time compared other machine learning method as e.g., artificial neural networks (cf. [5, 9]). This feature promises a suitability for real-time applications as digital twins. For the decision tree the input domain is split into multiple regions so that local average estimates of the output can be made. Consequently, a piecewise constant regression model is built in which a constant function is fitted for each region according to the local average to find a map between $P$ and $A$.

## 3. Numerical Model and Parametrisation

As an example, the structure shown in Fig. 2 is investigated numerically. It consists of a organo sheet as FRTP sheet and overmoulded reinforcing ribs.

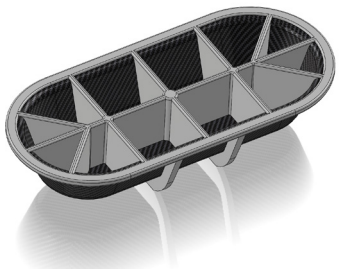

Fig. 2. Model of the investigated thermoplastic composite structure

First, the thermoforming of organo sheet is simulated by means of an injection moulding tool using the software LS-DYNA [12]. Based on the numerical results, a reduced order process model is obtained. The special characteristic of thermoforming in this study is that the process is carried out on an injection moulding tool. Accordingly, the tool has a maximum temperature of 80 °$C$. In addition, the punch contains cavities for the subsequent injection moulding process. This leads to an inhomogeneous temperature distribution in the organo sheet during forming. Since the local interface temperature is a significant factor for the developing bond strength of the overmoulded ribs, it has been analysed depending on the initial temperature of the organo sheet $T_o$, the mould temperature $T_m$ as well as the forming speed $v$.

### 3.1. Material and model

In the scope of the study, an organo sheet consisting of a polypropylene (PP) matrix (Tepex dynalite 104RG600(4)/47%) with a melting temperature of 163 °$C$ has been modelled. The thermoforming simulation consists of a coupled structural-thermal analysis using an explicit solver. The finite element model and corresponding boundary conditions are shown in Fig. 3.

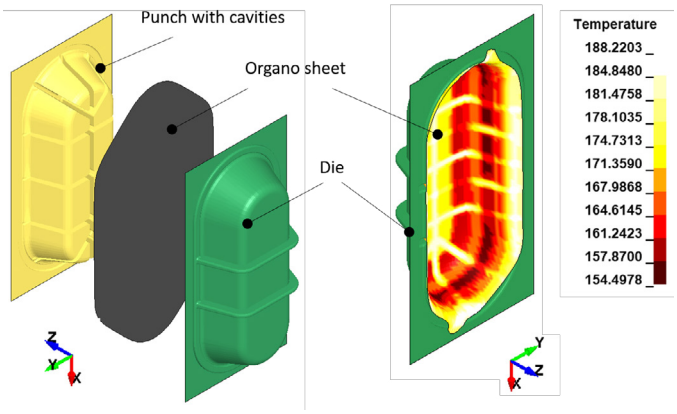


Fig. 3. Simulation model of the thermoforming process

The punch and die are modelled as rigid bodies without heat conduction and a homogeneous process temperature. For the organo sheet the material model *MAT_249_REINFORCED_THERMOPLASTIC has been applied. It is a special material model for fibre reinforced thermoplastics, where the fibres are described as anisotropic-hyperelastic and the matrix material as elastic-plastic. In addition, the mechanical properties can be modelled as a function of temperature [13].

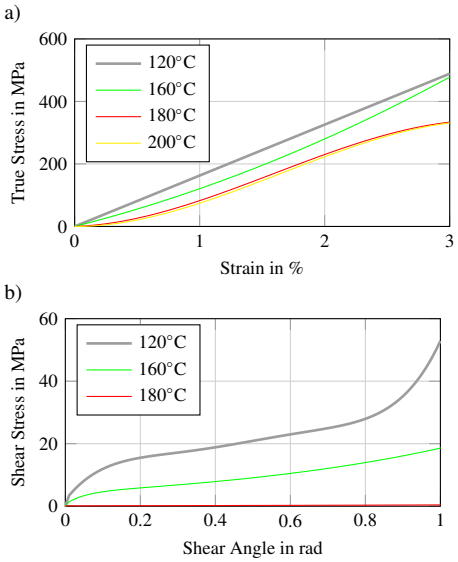


Fig. 4. Stress vs. strain (a) and shear stress vs. shear angle (b) of the organo sheet for different elevated temperatures

Accordingly, the stress-strain-curves of the organic sheet in the two main fibre directions 0°/90° and the specification of the shear stress as a function of the shear angle in ± 45° depicted in Fig. 4 are required as input.

Therefore, the corresponding parameters were determined by means of a tensile test according to DIN EN ISO 527-1/4 and a picture frame test according to DIN EN ISO 20337. Detailed information on the evaluation and modelling of the thermo-mechanical material properties can be found in [14]. In addition, the thermal material model *MAT_T01_THERMAL_ISOTROPIC is used to capture the thermal properties. All remaining thermal and mechanical properties of the organo sheet are summarised in Table 1.

Table 1. Thermal and mechanical properties of organo sheet

| Parameter | Symbol | Value |
|---|---|---|
| Density | $\rho$ | 1.69 $g\,cm^{-3}$ |
| Young's Modulus | $E_{matrix}$ | 3.0 $MPa$ |
| Poisson's ratio | $\nu$ | 0.4 |
| Locking angle | $\gamma$ | 1.25 $rad$ |
| Thermal conductivity | $\lambda$ | 0.22 $W\,m^{-1}\,K^{-1}$ |
| Heat capacity | $c_p$ | 1.7 $J\,g^{-1}\,K^{-1}$ |
| Heat transfer coefficient | $h$ | 510 $W\,m^{-2}\,K^{-1}$ |

### 3.2. Numerical Design of Experiments

In terms of the parametric study, the sensitivity of the local temperature distribution of the organo sheet is numerically investigated as a function of three different input parameters, which can be varied on the process side. A Latin Hypercube sampling (LHS) is applied for the numerical design of experiments. LHS is a statistical method for generating a near-random sample of parameter values from a multidimensional distribution.

Accordingly, the initial temperature of the organo sheet varies between $160\,°C \leq T_o \leq 220\,°C$, the tool temperature between $30\,°C \leq T_m \leq 80\,°C$ and the forming speed between $60\,mm\,min^{-1} \leq v \leq 600\,mm\,min^{-1}$. A total of 90 simulations with different parameter combinations are carried out in a batch process. For the reduced order model the temperature distribution in the final step of the forming process is evaluated. The resulting temperature field is referred to as snapshot.

## 4. Numerical Results

In this section, the convergence and accuracy of the reduced solution is investigated. The thermoforming model depicted in Fig. 3 yields 90 snapshots of the final temperature distribution. Exemplary, the resulting temperature distribution of the thermoformed organo sheet for specific parameter sets is shown in Fig. 5. Since each snapshot yields a slightly different forming result, the final temperature profile is projected onto the initial blank geometry. This provides a better comparability and overview of the results.

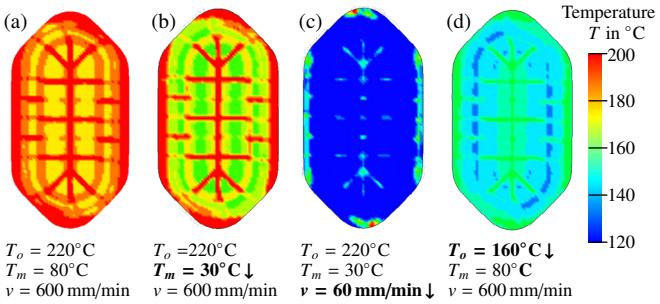


Fig. 5. Exemplary results of the temperature profile $T$ after thermoforming for a reference with the highest process parameters (a), for the lowest mould temperature $T_m$ (b), slowest forming speed $v$ (c) and lowest initial temperature of the organo sheet $T_o$ (d)

Fig. 5(a) shows the result with the highest process parameters, which is considered to be the reference sample. To analyse the influence of the individual parameters, each process parameter was reduced to its minimum value in the LHS and compared to the reference solution. For each of the parameter sets, the temperature profiles in Fig. 5 show the pattern of the injection moulding cavities of the die and punch. In the areas where contact between tool and organo sheet occurs, the organo sheet interface is cooling down considerably. In the reference sample Fig. 5(a) as well as in Fig. 5(b), a temperature above 200°C is observed in the areas along the cavities that represent the interface. The interface area does not cool down below melting temperature, since there is no contact with the colder mould in this area. However, the temperature gradient increases as the mould temperature decreases. In Fig. 5(c) and Fig. 5(d), the interface area is below or in the range of the melting temperature, thus it can be assumed that the polymer has completely or partially solidified. In Fig. 5(c), a significantly large temperature gradient occurs. In summary, both the forming speed and the initial temperature of the organo sheet are the main factors influencing the interface temperature and will subsequently influence the part quality.

### 4.1. Proper Orthogonal Decomposition

The solution of the eigenvalue problem is displayed in Fig. 6. The resulting normalised eigenvalues are plotted in descending order.

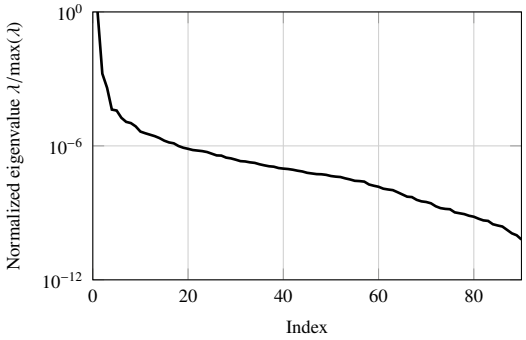


Fig. 6. Normalised eigenvalues $\lambda$ in descending order

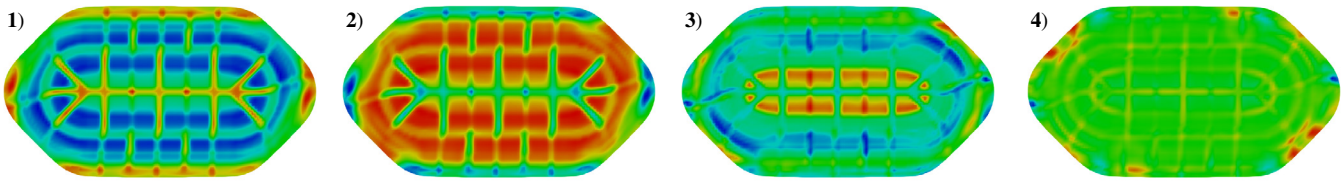


Fig. 7. Illustration of the spatial POD modes no. 1-4

Here, it can be observed that the relative value decreases very fast. The eigenvalues $\lambda_2(0.0017)$ and $\lambda_3(0.0004)$ are already of magnitudes smaller than $\lambda_1$. This implies a fast convergence of the POD. In Fig. 7, the first four spatial modes of the reduced solution (1) are shown.

Mathematically, these modes represent the orthogonal basis of the reduced solution space. Interpreting the physical meaning of the values shows a strong correlation between the mode and the resulting temperature profile depicted in Fig. 5. Consequently, combining these modes in the series expansion will always yield solutions that are consistent with the boundary conditions of the underlying physical problem. Especially the shape of the first mode is qualitatively similar to the temperature field, which underlines its major influence on the reduced solution (cf. Fig. 6). Similarly, for the second and third mode, the profile determined by the cavities is recognised. Together with the computed weighting functions, a sufficient number of spatial modes yield the reproduction of the full-scale solution.

In order to evaluate the prediction quality as a function of $k$, the error $\eta = \|\mathbf{U}_{red} - \mathbf{U}\|/\|\mathbf{U}\|$ is computed. It yields the relative error for each sample. In Fig. 8, the convergence behaviour of the POD approximation is shown. The relative error is plotted over the number of modes $k$ used in the approximation.

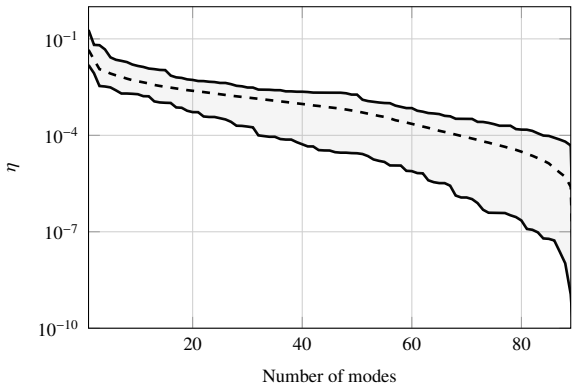


Fig. 8. Convergence behaviour of the POD

The range of the error is bounded by the error's maximum and minimum over all samples. The dotted line represents the mean error. From this graph, the number of samples needed to obtain a sufficient approximation of the results can be estimated. In this example, a mean error below 0.001 is achieved with approximately 40 modes. For ensuring in any case an error less than 0.001 at least 60 modes are necessary. Note that in this example the results reproduced by POD are all contained in the snapshots. Hence, using all available modes will always lead to an error in the range of the computer accuracy.

### 4.2. Machine Learning

In contrary to the concept described in [5], where machine learning methods are deployed for developing surrogate models directly from the FEA results, the intermediate step of a POD reduces the amount of data for the machine learning.

For the sake of completeness, the training is obtained for all 90 snapshots and modes. In practical applications the number of modes $k$ considered in the reduced model, can be chosen smaller according to the convergence of the POD (cf. Fig. 8), which would further reduce the amount of data. Since the spatial modes are not affected by the machine learning-based computation of weighting coefficients, the physical boundary conditions of the reduced model are preserved and only the map between process parameters and the weighting function is modelled as a black box. A decision tree is utilised for predicting the matrix of weighting functions $A$ by means of the individual process settings $P$. In Fig. 9, the relative error $\eta$ is depicted for samples with weighting coefficients determined by decision tree.

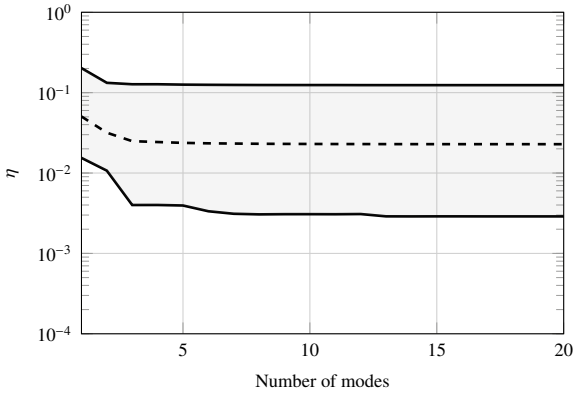


Fig. 9. Convergence behaviour of the POD using machine learning predicted weighting coefficients

Here, only for the first three modes show a significant improvement of the approximation. The addition of more modes yields only a small further improvement. The error remains almost constant for 10 modes and more. Even though a minimum error of up to 0.003 is possible, the maximum error convergences to a constant value of 0.124, which is too large for the application as digital twin. The mean error however implies with 0.023 that a suitable approximation is possible. In order to illustrate the convergence behaviour, the weighting coefficients and corresponding predictions for $a_1$ and $a_{20}$ are depicted in Fig. 10.

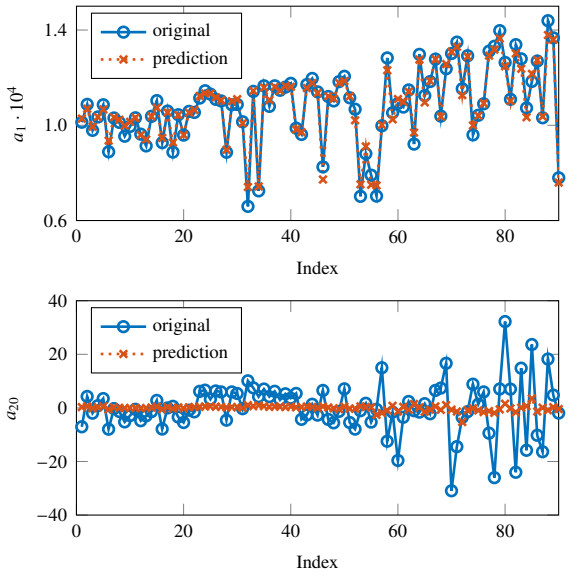


Fig. 10. Comparison of the weighting coefficients computed from POD and predicted with machine learning

The prediction of $a_1$ matches very well the originally computed values from POD. Regarding the prediction for $a_{20}$, it can be seen that the decision tree yields a nearly constant function around 0, whereas the original coefficient oscillates between −40 and 40. However, the absolute value of $a_{20}$ is magnitudes smaller than $a_1$. Hence, the absolute value of the weighting coefficients is smaller for the higher modes and therefore their influence on the reduced solution is also smaller.

## 5. Concluding Remarks

The interface bond strength in overmoulded thermoplastic composites is the most critical factor for the structural integrity. A sufficient bond strength has to be ensured during the design phase considering the influence of the manufacturing process. In the presented approach, the interface temperature of a FRTP sheet (organo sheet), as main influence parameter for the bond strength, is predicted by means of a numerical design of experiments, POD and decision trees. The numerical design of experiments shows that the initial temperature of the organo sheet and the forming speed have the largest influence on the temperature distribution. The resulting digital twin yields a physics-based online feasible surrogate model, that can be used to optimise the part design, as input for the design of the subsequent injection moulding or as virtual quality gate during operation. The error analysis shows a mean approximation error of 0.023, which is a suitable approximation. However, the analysis shows further that deviations of more than 10% occur in the predicted results. Especially the weighting coefficients of the higher POD modes are not well approximated, which yields further research questions concerning suitable machine learning methods and parametrisation. However, with each new development cycle, the amount of simulation data and consequently the process knowledge increases. By considering also the injection moulding process in the digital twin, the whole process chain can be captured. This additionally requires a fast mapping procedure between thermoforming and injection moulding mesh.

## Acknowledgments

This research and results published are based on the research program Mobilise funded by the Ministry of Science and Culture of Lower Saxony and the Volkswagen Foundation and the IGF-Project “Integrated process simulation of thermoforming and injection moulding“ of the European Research Association for Sheet Metal Working (EFB e.V.) funded by the Federal Ministry of Economics and Energy (BMWi) under the funding number 20524N of the German Federation of Industrial Research Associations (AiF). The authors gratefully acknowledge this financial support.

## References

[1] Bouwman, M., Donderwinkel, T., Krämer, E., Wijskamp, S., Costa, S.F., 2016. Overmoulding–An Integrated Design Approach for Dimensional Accuracy and Strength of Structural Parts. ITHEC Proceedings .

[2] Liebsch, A., Kupfer, R., Krahl, M., Haider, D.R., Koshukow, W., Gude, M., 2018. Adhesion studies of thermoplastic fibre-plastic composite hybrid components-Part 1: thermoplastic-thermoplastic-composites. Hybrid Materials and Structures .

[3] Akkerman, R., Bouwman, M., Wijskamp, S., 2020. Analysis of the Thermoplastic Composite Overmolding Process: Interface Strength. Frontiers in Materials 7. doi:10.3389/fmats.2020.00027.

[4] Giusti, R., Lucchetta, G., 2020. Modeling the Adhesion Bonding Strength in Injection Overmolding of Polypropylene Parts. Polymers 12. doi:10.3390/polym12092063.

[5] Hürkamp, A., Gellrich, S., Ossowski, T., Beuscher, J., Thiede, S., Herrmann, C., Dröder, K., 2020. Combining Simulation and Machine Learning as Digital Twin for the Manufacturing of Overmolded Thermoplastic Composites. Journal of Manufacturing and Materials Processing 4, 92. doi:10.3390/jmmp4030092.

[6] Thiede, S., Juraschek, M., Herrmann, C., 2016. Implementing Cyber-physical Production Systems in Learning Factories. Procedia CIRP 54, 7–12. doi:10.1016/j.procir.2016.04.098.

[7] Chinesta, F., Cueto, E., Abisset-Chavanne, E., Duval, J.L., Khaldi, F.E., 2018. Virtual, Digital and Hybrid Twins: A New Paradigm in Data-Based Engineering and Engineered Data. Archives of Computational Methods in Engineering doi:10.1007/s11831-018-9301-4.

[8] Berkooz, G., Holmes, P., Lumley, J.L., 1993. The proper orthogonal decomposition in the analysis of turbulent flows. Annual review of fluid mechanics 25, 539–575.

[9] Swischuk, R., Mainini, L., Peherstorfer, B., Willcox, K., 2019. Projection-based model reduction: Formulations for physics-based machine learning. Computers & Fluids 179, 704–717. doi:10.1016/j.compfluid.2018.07.021.

[10] Hürkamp, A., Lorenz, R., Behrens, B.A., Dröder, K., 2019. Computational Manufacturing for Multi-Material Lightweight Parts. Procedia CIRP 85, 102–107. doi:10.1016/j.procir.2019.09.041.

[11] Sirovich, L., 1987. Turbulence and the dynamics of coherent structures. I. Coherent structures. Quarterly of Applied Mathematics 45, 561–571. doi:10.1090/qam/910462.

[12] Livermore Software Technology Corporation, 2018. LS-DYNA.

[13] LST, 2020. LS-DYNA keyword user’s manual - Volume II. r12 ed. 2020. Livermore Software Technology Corporation .

[14] Behrens, B.A., Chugreev, A., Wester, H., 2019. Experimental and numerical characterization method for forming behavior of thermoplastics reinforced with woven fabrics. Procedia Manufacturing 29, 443–449. doi:10.1016/j.promfg.2019.02.160.